The distribution of the maximum of independent resetting Brownian motions

Alexander K. Hartmann,[1] Satya N. Majumdar,[2] and Grégory Schehr[3]

[1]*Institut für Physik, Universität Oldenburg, 26111 Oldenburg, Germany*
[2]*LPTMS, CNRS, Univ. Paris-Sud, Université Paris-Saclay, 91405 Orsay, France*
[3]*Sorbonne Université, Laboratoire de Physique Théorique et Hautes Energies,*
CNRS UMR 7589, 4 Place Jussieu, 75252 Paris Cedex 05, France

The probability distribution of the maximum M_t of a single resetting Brownian motion (RBM) of duration t and resetting rate r, properly centred and scaled, is known to converge to the standard Gumbel distribution of the classical extreme value theory. This Gumbel law describes the typical fluctuations of M_t around its average $\sim \ln(rt)$ for large t on a scale of $O(1)$. Here we compute the large-deviation tails of this distribution when $M_t = O(t)$ and show that the large-deviation function has a singularity where the second derivative is discontinuous, signalling a dynamical phase transition. Then we consider a collection of independent RBMs with initial (and resetting) positions uniformly distributed with a density ρ over the negative half-line. We show that the fluctuations in the initial positions of the particles modify the distribution of M_t. The average over the initial conditions can be performed in two different ways, in analogy with disordered systems: (i) the annealed case where one averages over all possible initial conditions and (ii) the quenched case where one considers only the contributions coming from typical initial configurations. We show that in the annealed case, the limiting distribution of the maximum is characterized by a new scaling function, different from the Gumbel law but the large-deviation function remains the same as in the single particle case. In contrast, for the quenched case, the limiting (typical) distribution remains Gumbel but the large-deviation behaviors are new and nontrivial. Our analytical results, both for the typical as well as for the large-deviation regime of M_t, are verified numerically with extremely high precision, down to 10^{-250} for the probability density of M_t.

I. INTRODUCTION

Consider a random searcher on a line whose dynamics is characterized by a stochastic process $x(t)$, starting say at the origin $x = 0$. Let M denote the location of a fixed target, see Fig. (1). **ALEX:** *Usually figure numbers are without brackets (), they are just for equations. Is it required here? If not, change everywhere.* How long will the searcher take to find the target? This is a key fundamental question for any search process. A quantity that plays a central role is the survival probability $Q(M, t)$ of the target up to time t, i.e., the probability that the target is not found by the searcher up to time t. The actual time to find the target is a random variable known as the first-passage time. The probability distribution function (PDF) $P(t_f|M)$ of the first-passage time is very simply related to the survival probability by the relation

$$Q(M, t) = \text{Prob.}\,[t_f \geq t] = \int_t^\infty P(t_f|M)\, dt_f\,, \tag{1}$$

which simply follows from the fact that if the target survives up to t, it must be found by the searcher only after t, i.e., $t_f \geq t$. Taking derivative with respect to t relates the survival and the first-passage probabilities

$$P(t_f|M) = -\frac{\partial}{\partial t} Q(M, t)\Big|_{t=t_f}\,. \tag{2}$$

Search processes are ubiquitous in nature [1–3]: animals searching for food, proteins searching for a DNA site to bind, chemicals diffusing and searching for other constituents to react, debugging schemes searching for a bug in a computer program, randomized algorithms searching for a global minimum in a high dimensional landscape and many others. Survival probability and the associated first-passage time distribtion is a key concept in random search processes with many applications [4–13]. It can be considered as a cost function for a search process. The efficiency of a search process is enhanced by minimizing the survival probability of the target. Given the ubiquity of search processes, the survival probabilty $Q(M, t)$ or the associated first-passage probability $P(t_f|M)$ has been studied for more than 100 years across disciplines: in mathematics, physics, chemistry, biology and computer science [14–19]. In physics of nonequilibrium many-body systems, the survival probability or 'persistence' also appears as a key quantity that characterizes the history dependence of the underlying stochastic systems [18].

Another, a priori unrelated, subject that has also been widely studied with applications ranging from sports, climate science, finance all the way to physics of disordered systems is the extreme value statistics (EVS) [20–22], for a recent pedagogical review on EVS, see Ref. [24]. In EVS, one typically looks at a time-series, for example the temperature or rainfall data in a given weather station or the price of a stock, and records the maximum (or minimum) M_t of the process or the time-series up to time t. The histogram of M_t gives access to its PDF $P(M, t)$. The statistical behavior of M_t, encoded in $P(M, t)$, gives important informations about the extreme fluctuations and play a crucial role, e.g., in analysing data for global warming [25]. When the underlying time-series is completely uncorrelated, the EVS is well understood from the classical literature in statistics and mathematics [20, 23] and $P(M, t)$, appropriately centered and scaled, is usually governed by one of the three well known extreme value distributions, known as the Gumbel, the Fréchet and the Wiebull class [24]. However, much less is understood about the EVS when the underlying time-series is correlated [24].

These two subjects, namely the survival probability and the EVS, are actually very closely related. To see this, consider again the one dimensional situation and let the process $x(t)$ that represents the motion of the searcher in our underlying time-series, with initial value $x(0) = 0$. Let M_t denote the maximum achieved by this process up to time t, i.e.,

$$M_t = \max_{0 \leq \tau \leq t} \left[\{x(\tau)\}\right]\,. \tag{3}$$

Then the cumulative distribution function (CDF) of the maximum is defined as

$$\text{Prob.}[M_t \leq M] = \int_0^M P(M', t)\, dM'\,, \tag{4}$$

where $P(M, t)$ is the PDF of M_t. However, if the maximum M_t is less than M, this event is equivalent to the probability that all positions of the searcher $\{x(\tau)\}$ up to t must be less than M (see Fig. (1)). In other words, this is precisely the probability that the target at M is not touched/found by the process up to t, i.e., the survival probability $Q(M, t)$ of the target up to time t. This establishes a precise and general relation between the EVS and survival probability

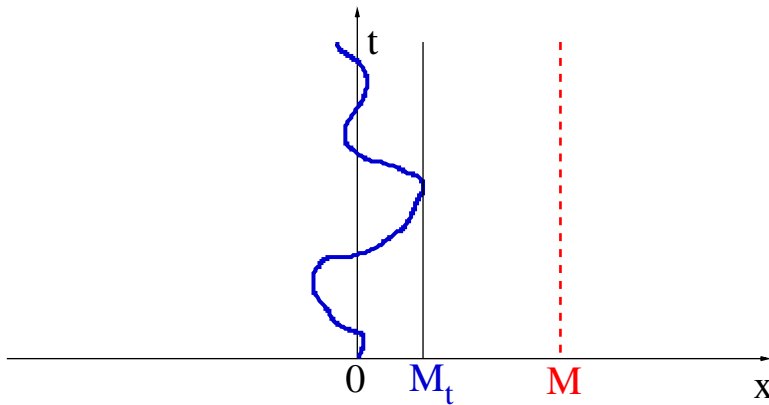$$\text{Prob.}[M_t \leq M] = \int_0^M P(M', t)\, dM' = Q(M, t)\,. \tag{5}$$

FIG. 1. Schematic trajectory of a stochastic search process $x(t)$, starting from $x(0) = 0$, with global maximal value M_t up to time t. A fixed target, shown by vertical dashed (red) line, is located at M. The survival probability $Q(M, t)$ of the target up to time t is exactly the probability of the event $M_t \leq M$, as in Eq. (5).

Thus, if we know the survival probability $Q(M, t)$, the PDF of the maximum M_t is simply obtained from (5) by taking a derivative with respect to M

$$P(M, t) = \frac{\partial}{\partial M} Q(M, t). \tag{6}$$

To summarize, the survival probability $Q(M, t)$ has two arguments M and t. Taking a derivative with respect to M, as in Eq. (6), provides the PDF of the maximum M_t of the process up to time t. In contrast, taking the negative of the derivative of $Q(M, t)$ with respect to t, as in Eq. (2), provides the PDF of the first-passage time to the target at M.

So far the discussion has been for any arbitrary random search process in one dimension. We now focus on a specific random search process that has created much interest over the last decade is known as the resetting Brownian motion (RBM) [26–28]. In this simple model, the trajectory of the searcher performs an ordinary Brownian motion, starting from its initial position at 0, during a random time interval τ, distributed via $p(\tau)$. At the end of the interval, the trajectory is reset to the starting position and a new random time interval is chosen from $p(\tau)$ during which the searcher undergoes free diffusion and so on. When the interval between resettings is distributed via

$$p(\tau) = r \, e^{-r\,\tau}, \tag{7}$$

the model is called Poissonian resetting where the Brownian motion resets to its starting position at a constant r [26]. But other variants, such as 'periodic' or 'sharp' restart where $p(\tau) = \delta(\tau - T)$ or power-law distributed $p(\tau)$ have also been studied [29–33].

Here we will focus on simple Poissonian resetting with rate r, mainly because this model is simple and has a rather nice analytical structure. A nonzero resetting rate r has two major effects [26]: (i) by breaking the detailed balance, it drives the system into a nonequilibrium stationary state where the position distribution is typically non-Gaussian at long times and (ii) in the presence of a target at fixed M and with the RBM starting and resetting at 0, the mean first-passage time (MFPT) to the target, as a function of the resetting rate r, achieves a minimum at an optimal value r^*. The existence of an optimal r^* makes the RBM an efficient search process [26–28, 30, 32, 34–41] and confirms the scenario that when searching for a target in vain for a while, it is better to restart the search process: the rational being that the searcher may explore a different pathway searching for the target, thus expediting the search process. However, the existence of an optimal r^* is not always guaranteed. Several models have been studied, where by varying a parameter in the underlying process, the optimal r^* may undergo a phase transition, becoming zero beyond a critical value of the parameter [32, 34, 36, 42–52]. Stochastic resetting has created much interest across fields in the last decade (for recent reviews see Refs. [53–55]). Various observables for diffusion with stochastic resetting have also been measured in experiments using holographic optical tweezers in one and two dimensional optical traps [56–59].

The purpose of this chapter is to illustrate the complementary perspectives of the same observable from two different fields, i.e., search processes and the EVS, within the simple model of a resetting Brownian motion as the search process.

In Section II, we will explore the observable $Q_r(M,t)$ denoting the survival probability of a target placed at M, in the presence of a single searcher whose dynamics is governed by the RBM, starting and resetting at the origin with rate r. As mentioned earlier, $Q_r(M,t)$ can alternatively be interpreted as the CDF of the maximum M_t of the RBM (without any target) up to time t. The Laplace transform (with respect to time t) of $Q_r(M,t)$ was already computed exactly in Ref. [26]. However, it turns out that the exact Laplace inversion is difficult and interesting behaviors of $Q_r(M,t)$ for different scales of M in real time t are actually hidden in the Laplace transform. Treating $\partial_M Q_r(M,t) = P_r(M,t)$ as the PDF of the maximum M_t (see Eq. (6)), one can extract the mean $\langle M_t \rangle$ and its variance explicitly and they have been used in many applications. These include, for instance, computing the statistics of the number of distinct sites visited by a resetting random walker on a one dimensional lattice [60], computing the mean perimeter and the mean area of the convex hull of a two dimensional RBM [61], and also calculating the distribution of the time at which the maximum occurs in the stationary state of an RBM [62, 63]. Similarly, higher moments of M_t can also be extracted analytically [64]. However, extracting the full extreme-value distribution $Q_r(M,t)$ for all M from its Laplace transform is highly nontrivial. Our first goal in Section II would be to analyse this Laplace trasnform carefully to bring out the late time behavior of $Q_r(M,t)$ for all M. In particular, treating $Q_r(M,t)$ as the CDF of the maximum M_t brings out new interesting scales of M_t. We will see that while the typical fluctuations of M_t are of $O(\ln t)$ for large t, there is an interesting large-deviation tail when $M \sim O(t)$ where the associated rate function undergoes a second-order dynamical phase transition. We will analyse $Q_r(M,t)$ in different regions of the $M - t$ plane and explore its scaling behaviors.

In Section III, we will consider a generalization of the single particle system to a many-particle scenario. Here we will have N particles distributed uniformly with density ρ on the left half of the origin at $t = 0$, with the target located at $M \geq 0$. Each particle undergoes resetting Brownian motions independently, i.e., the i-th particle starts at the initial random position x_i and undergoes diffusion and resetting to its own initial position x_i. The process ends when the target is found by any one of the N particles. Let $M_t(i)$ denote the maximum, up to t, of the i-th particle. Clearly, $M_t(i)$'s are independent random variables. Then the global maximum

$$M_t = \max_{1 \leq i \leq N} [M_t(i)] , \tag{8}$$

represents the maximum of a set of N independent, but *not identically* distributed variables. The different initial and resetting positions make the variables $M_t(i)$ non-identically distributed. We will see that this has interesting implications for the extreme-value statistics. In addition, the behavior of the survival probability or the EVS depends strongly on how the averaging over the initial positions is performed. If one averages the survival probability over all possible initial conditions with equal weight, this is called *annealed* survival probability, in analogy with disordered systems. In contrast, when one averages only over typical initial configurations (regular equidistant positions with typical interparticle separation $1/\rho$) and ignores the rest, the corresponding survival probability is *quenched*, again in analogy with disordered systems. We will see that the annealed and the quenched survival probabilities have rather different behaviors. This also has interesting significance from the perspective of extreme-value statistics as will be illustrated. Moreover, in the two cases, we will also explore both the typical as well as the large-deviation regimes of the survival probability as a function of M for large t. We note that in Ref. [26], the survival probability for both the annealed and the quenched cases were analysed, but only for $M = 0$, i.e., when the target is fixed at the origin. However, to understand how the extreme M_t behaves, we need to analyse the survval probability for general $M \geq 0$. Thus, the results for general $M \geq 0$ presented in this chapter are original and go beyond Ref. [26].

In Section IV, we will verify our analytical predictions via high-precision numerical simulations. Finally, we will conclude with some perspectives in Section V.

II. SINGLE PARTICLE CASE

We start with a single RBM, starting and resetting at the origin with rate r, with a target fixed at M. Let M_t be the maximum of this RBM up to time t, see Fig. 1. As mentioned in the introduction, the survival probability $Q_r(M,t)$ of the target up to time t is exactly the CDF of the random variable M_t, see Eq. (5). Thus $Q_r(M,t)$ has two alternative interpretations. When one thinks of it as the cumulative distribution of the maximum, one thinks $Q_r(M,t)$ as a function of M for a fixed t. In contrast, when one thinks of $Q_r(M,t)$ as the survival probability of a fixed target located at M, one is more interested in determining how the survival probability decays as a function of time t, for fixed M. Here, we will therefore analyse $Q_r(M,t)$ in the $M - t$ plane for $M \geq 0$ and $t \geq 0$. In the first case, we will fix t and observe $Q_r(M,t)$ as a function of M where it has the interpretation of a cumulative probability and increases from 0 at $M = 0$ to 1 as $M \to \infty$, for any fixed t. In the second case, we will fix M and study how $Q_r(M,t)$ decays as a function of time t.

The survival probability $Q_r(M,t)$, or instead its Laplace transform, can be easily computed using the renewal property of the RBM [26, 53]. Let $Q_0(M,t)$ denote the survival probability of an ordinary Brownian motion without

resetting. This Brownian motion starts at the origin and diffuses with a diffusion constant D in the presence of a fixed target at $M \geq 0$. This survival probability can be easily computed by solving the diffusion equation with an absorbing boundary condition at M and this well known result reads [15, 17, 18]

$$Q_0(M,t) = \text{erf}\left(\frac{M}{\sqrt{4Dt}}\right) , \tag{9}$$

where $\text{erf}(z) = (2/\sqrt{\pi}) \int_0^x e^{-u^2} du$ is the error function. For large times, it decays as a power law, $Q_0(M,t) \sim M/\sqrt{\pi D t}$. In the presence of resetting with a nonzero rate $r > 0$, one can write the survival probability $Q_r(M,t)$ in terms of $Q_0(M,t)$ via the renewal equation [53]

$$Q_r(M,t) = e^{-rt}Q_0(M,t) + r \int_0^t d\tau\, e^{-r\tau} Q_r(M,t-\tau) Q_0(M,\tau) . \tag{10}$$

This equation can be interpreted as follows. The first term corresponds to the event when there is no resetting in the full interval $[0,t]$ and the process is then an ordinary Brownian motion that needs to survive up to time t. The probability of this event is, from Eq. (7), the probability $\int_t^\infty p(\tau)d\tau = e^{-rt}$ that no resetting occurs up to time t, times the survival probability $Q_0(M,t)$, explaining the first term in (10). The second term corresponds to the events with one or more resettings. In this case let the last resetting event before t occur at time $t - \tau$. In the interval $[t-\tau,t]$ there is no resetting, preceded by one resetting event at time $t - \tau$: this joint event occurs with probability $p(\tau)d\tau = r\,d\tau e^{-r\tau}$. During this interval $[t-\tau,t]$, the process evolves as a free Brownian motion and its survival probability is simply $Q_0(M,\tau)$. But one needs to ensure also that the process (with resetting) did not cross M during $[0,t-\tau]$, which occurs with a probability $Q_r(M,t-\tau)$. Since these events are independent due to the Markov nature of the process, we take the product of these three probabilities and integrate over τ from 0 to t, leading to the second term in Eq. (10). Let us now define the Laplace transform

$$\tilde{Q}_r(M,s) = \int_0^\infty e^{-st} Q_r(M,t)\, dt . \tag{11}$$

Since Eq. (10) has a convolution structure in time, it is natural to take its Laplace transform which then leads to

$$\tilde{Q}_r(M,s) = \frac{\tilde{Q}_0(M,r+s)}{1 - r\tilde{Q}_0(M,r+s)} . \tag{12}$$

Using the expression of $Q_0(M,t)$ in Eq. (9), one has

$$\tilde{Q}_0(M,s) = \int_0^\infty e^{-st} Q_0(M,t)\, dt = \frac{1}{s}\left(1 - e^{-\sqrt{s/D}\,M}\right) . \tag{13}$$

Substituting this in Eq. (12) gives the well known result [26, 53]

$$\tilde{Q}_r(M,s) = \int_0^\infty e^{-st} Q_r(M,t)\, dt = \frac{1 - e^{-\sqrt{\frac{r+s}{D}}\,M}}{s + r\,e^{-\sqrt{\frac{r+s}{D}}\,M}} . \tag{14}$$

Inverting this Laplace transform formally, we get

$$Q_r(M,t) = \int_\Gamma \frac{ds}{2\pi i}\, e^{st}\, \frac{1 - e^{-\sqrt{\frac{r+s}{D}}\,M}}{s + r\,e^{-\sqrt{\frac{r+s}{D}}\,M}} \tag{15}$$

where Γ is a Bromwich contour which has to pass to the right of all singularities of the integrand. In principle, this is an exact expression of the survival probability, or equivalently that of the CDF of M_t, valid for all M and all t. In the rest of this section, we will analyse the behavior of $Q_r(M,t)$ in different regions of the $M - t$ plane, see Fig. (2). In the following subsection, we analyse $Q_r(M,t)$ for fixed t as a function of M – here the interpretation of $Q_r(M,t)$ is the cumulative distribution of the random variable M_t. In the next subsection, we will analyse $Q_r(M,t)$ as a function of t for fixed M – this has the interpretation of the survival probability.

A. Probability distribution of the maximum

Here, we interpret $Q_r(M,t)$ as the CDF of the maximum M_t up to time t of the RBM, starting and resetting at the origin with rate r. It is also natural to consider the associated PDF $P_r(M,t) = \partial_M Q_r(M,t)$. Using Eq. (14), the
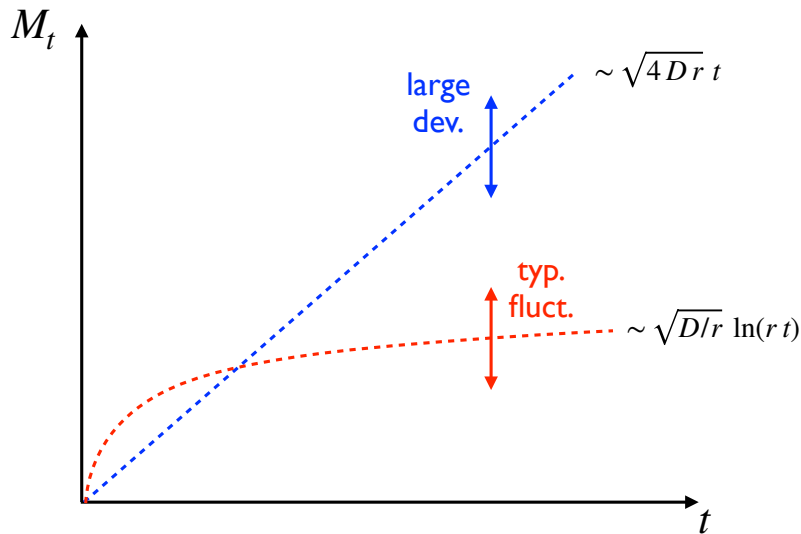
FIG. 2. A schematic representation of the two time scales associated with the fluctuations of the maximum M_t up to time t for a resetting Brownian motion. For a fixed but large t, while the typical fluctuations scale as $\ln(rt)$ (shown by the red dashed curve), the large deviations scale linearly with t as shown by the blue dashed line.

Laplace transform of the PDF of M_t is then given by

$$\tilde{P}_r(M,s) = \frac{\partial}{\partial M} Q_r(M,s) = \frac{(s+r)^{3/2}}{\sqrt{D}} \frac{e^{-\sqrt{\frac{r+s}{D}} M}}{(s + r\, e^{-\sqrt{\frac{r+s}{D}} M})^2} \ . \tag{16}$$

Therefore $P_r(M,t)$ is given by the Bromwich integral

$$P_r(M,t) = \int_\Gamma \frac{ds}{2\pi i} e^{s\,t} \frac{(s+r)^{3/2}}{\sqrt{D}} \frac{e^{-\sqrt{\frac{r+s}{D}} M}}{(s + r\, e^{-\sqrt{\frac{r+s}{D}} M})^2} \ , \tag{17}$$

where Γ is a Bromwich contour.

We first fix t to be large and consider $P_r(M,t)$ in Eq. (17) as a function of M. To analyse this integral, we need to examine the singularities of the integrand in the complex s-plane and make sure that the vertical Bromwich contour Γ is to the right of all the singularities. The integrand clearly has a branch cut at $s = -r$ and also a double pole at $s = s^*$ where s^* is given by the root of the equation

$$s + r\, e^{-\sqrt{\frac{r+s}{D}} M} = 0 \ . \tag{18}$$

In the limit of large M, we expect $|s^*| \ll 1$. Consequently we have, from Eq. (18), to leading order for large M,

$$s^* = -r\, e^{-\sqrt{\frac{r}{D}} M} \ . \tag{19}$$

We also notice that the integrand in (17) admits, for large t and large M, a saddle point s_1 which is obtained by minimizing $(s\,t - \sqrt{(r+s)/D}\, M)$, leading to

$$s_1 = -r + \frac{1}{4D} \left(\frac{M}{t} \right)^2 \ . \tag{20}$$

Therefore, when $s_1 > s^*$, we can deform the Bromwich contour to pass through s_1 and pick up the dominant contribution for large t – in this case we do not need to consider the contribution from the pole. In contrast, if $s_1 < s^*$, the dominant contribution will come from the pole at s^*. From (19), we see that for large M, the pole s^* is essentially close to zero, $s^* \approx 0$. Thus, from Eq. (20), it follows that $s_1 > s^* \approx 0$ if $M > M_c(t)$ where

$$M_c(t) = \sqrt{4\,D\,r}\, t \ . \tag{21}$$

In contrast, when $M < M_c(t)$, the leading contribution comes from the pole. By evaluating the residue at this pole, one gets

$$P_r(M, t) \approx \sqrt{\frac{r}{D}} \, (rt) \, \exp\left[-\sqrt{\frac{r}{D}} \, M - rt \, e^{-\sqrt{\frac{r}{D}} M}\right] . \tag{22}$$

Clearly, this is of order $O(1)$ when $M \sim \sqrt{D/r} \, \ln(r\,t)$.

Hence we clearly see that there are two scales that characterise the fluctuations of M_t, namely when $M_t \sim \ln(r\,t)$ and $M_t \sim t$. While the first one corresponds to the typical scale of fluctuations of M_t, the second one represents large deviations of M_t compared to its typical value. We now consider these two scales of fluctuations separately.

Typical fluctuations: In this case, the dominant contribution to the integral in Eq. (17) comes from the double pole at $s = s^*$, leading to the asymptotic form of the PDF $P_r(M, t)$ in Eq. (22). This can be expressed in a nice scaling form

$$P_r(M, t) \approx \sqrt{\frac{r}{D}} \, \mathcal{F}\left(\sqrt{\frac{r}{D}} \left(M - \sqrt{\frac{D}{r}} \ln(r\,t)\right)\right) , \tag{23}$$

where the scaling function $\mathcal{F}(v)$ has the Gumbel form

$$\mathcal{F}(v) = e^{-v - e^{-v}} , \tag{24}$$

which is normalised to unity, $\int_{-\infty}^{\infty} \mathcal{F}(v) \, dv = 1$. From this scaling form (23), it is clear that the PDF of M_t is peaked around the typical value $M_t \sim \sqrt{\frac{D}{r}} \ln(r\,t)$ and the fluctuations around this typical value is of order $O(1)$ for large t. In other words, one can express the random variable M_t as

$$M_t = \sqrt{\frac{D}{r}} \, (\ln(r\,t) + v) , \tag{25}$$

where v is a $O(1)$ random variable for large t, distributed via the Gumbel PDF $\mathcal{F}(v)$.

The result in Eq. (25) has a nice physical interpretation [53] in terms of extreme-value statistics (EVS) of independent and identically distributed (IID) random variables [24]. Consider the RBM without the target, starting and resetting at the origin. A typical trajectory of this RBM up to a large time t consists of a large number of intervals separated by resetting events. Since the resetting occurs with rate r, the number of such intervals in time t is typically $N_r = t/(1/r) = r\,t$. Within each interval labelled by $i = 1, 2, \cdots, N_r$, there is a local maximum of the displacement denoted by m_i. Clearly the global maximum M_t is given by

$$M_t = \max\{m_1, m_2, \cdots, m_{N_r}\} . \tag{26}$$

Since the m_i's belong to different resetting intervals, they are clearly independent of each other. To find the PDF of m_i, consider the i-th interval between resettings. Inside this interval, the motion is purely Brownian and the CDF of the maximum within this interval of length say τ is given by $\text{erf}\left(\frac{m_i}{\sqrt{4D\tau}}\right)$ as in Eq. (9). However, the interval duration τ itself is exponentially distributed via the PDF $p(\tau) = r\,e^{-r\tau}$. Averaging over this random duration, one gets the CDF of the maximum within a given interval as

$$\text{Prob.}\,[m_i \le m] = r \int_0^\infty e^{-r\tau} \, \text{erf}\left(\frac{m}{\sqrt{4D\tau}}\right) \, d\tau = 1 - e^{-\sqrt{r/D} \, m} , \tag{27}$$

where we used Eq. (13). Consequently, the PDF of m_i is given by

$$\text{Prob.}\,[m_i = m] = \sqrt{\frac{r}{D}} \, e^{-\sqrt{r/D} \, m} , \quad m \ge 0 . \tag{28}$$

Hence, M_t in Eq. (26) is the maximum of a set of $N_r = rt$ IID random variables, each distributed via the PDF in Eq. (28). Consequently, using the EVS of IID variables each with exonential distribution [24], one would expect that M_t will indeed scale as $\ln N_r = \ln(r\,t)$ with fluctuations of order $O(1)$ around it and in addition, the centered and scaled distribution will have the Gumbel from as in Eq. (24).

Large-deviation regime: Here we are interested in the large-deviation tail of $P_r(M, t)$ when $M = \mathcal{O}(t)$. In this limit, the saddle point s_1 is of order $O(1)$ from Eq. (20). If $M > M_c(t) = \sqrt{4D\,r}\,t$ given in Eq. (21), the saddle point
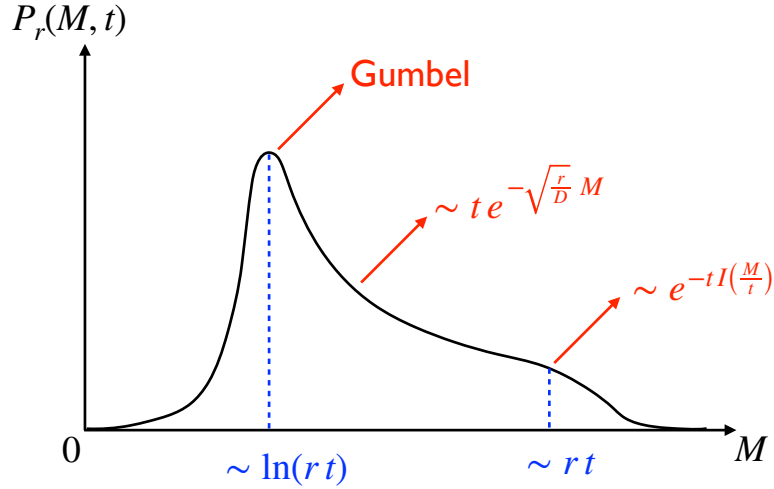
FIG. 3. A schematic plot of the PDF $P_r(M, t)$ of the maximum M_t as a function of M, for fixed but large t as in Eqs. (31) and (32). The two vertical dashed blue lines represent the typical and the large-deviation scales.

$s_1 > s^* \approx 0$. In this case, deforming the Bromwich contour through the saddle point, and performing the steepest descent analysis, we get

$$P_r(M, t) \approx e^{-r\,t - \frac{M^2}{4\,D\,t}} . \tag{29}$$

Thus so far, we have seen that there are two well separated scales of fluctuations of M_t, respectively of order $O(t)$ and order $O(\ln(r\,t))$, where the PDF takes very different forms given respectively in Eqs. (29) and (22). One may wonder what happens in the intermediate regime when $\ln t \ll M \ll t$. In this regime, the Gumbel form in Eq. (22) continues to hold but one can neglect the term $r\,t\,e^{-\sqrt{r/D}\,M}$ since $M \gg \ln(r\,t)$. Hence the approximate form of the PDF in this intermediate range reads

$$P_r(M, t) \approx \frac{r^{3/2}}{\sqrt{D}}\,t\,e^{-\sqrt{\frac{r}{D}}M} . \tag{30}$$

To summarise, the PDF of the maximum exhibits different behaviors in the three different regimes

$$P_r(M,t) \approx \begin{cases} \sqrt{\frac{r}{D}}\exp\left[-\sqrt{\frac{r}{D}}\left(M - \sqrt{\frac{D}{r}}\ln(r\,t)\right) - e^{-\sqrt{\frac{r}{D}}\left(M-\sqrt{\frac{D}{r}}\ln(r\,t)\right)}\right] & \text{for} \quad M = \mathcal{O}\left(\ln(r\,t)\right) \\[2ex] \frac{r^{3/2}}{\sqrt{D}}\,t\,e^{-\sqrt{\frac{r}{D}}M} \quad , \quad \text{for} \quad \ln r\,t \ll M \ll r\,t \\[2ex] e^{-r\,t - \frac{M^2}{4\,D\,t}} \quad , \quad \text{for} \quad M = \mathcal{O}(r\,t) \end{cases} \tag{31}$$

While the Gumbel behaviour in the first line corresponds to the typical trajectories with a large number of resettings, the last line corresponds to very rare trajectories that have undergone no reset up to time t. The intermediate regime corresponds to trajectories with few resets. The right tail of the intermediate regime and the left tail of the last regime can be combined into a single large-deviation form

$$P_r(M, t) \approx e^{-t\,I\left(\frac{M}{t}\right)} , \tag{32}$$

where

$$I(z) = \begin{cases} \sqrt{\frac{r}{D}}z \quad , \quad z \le z_c = \sqrt{4\,D\,r} \\[2ex] r + \frac{z^2}{4D} \quad , \quad z \ge z_c = \sqrt{4\,D\,r} . \end{cases} \tag{33}$$

Thus, the second derivative of $I(z)$ is discontinuous at $z = z_c$. In terms of the location of the maximum at time t, one sees that there is a "light cone" $M_c(t) = z_c\,t$ in the $M - t$ plane, such that for $M \le M_c(t)$, the typical behavior

of the maximum is established, while outside the "light cone" $M \geq M_c(t)$, the distribution of M is still atypical, corresponding to rare trajectories with no resetting. Indeed, this large-deviation form of $P_r(M, t)$ in Eq. (33) is exactly identical to the large-deviation form of the position distribution of the RBM [35]. The typical, intermediate and the large-deviation behaviors of $P_r(M, t)$ are summarized schematically in Fig. 3.

B. Survival probability

In this subsection, we consider $Q_r(M, t)$ as a survival probability, with a target fixed at M and analyse it as a function of time t. This means traversing the $M - t$ plane in Fig. (2) horizontally by increasing t at a fixed M.

We first consider the limit of large t, with M fixed but not necessarily large. In this case, the dominant behvaior of the integral in Eq. (15) emerges from the pole of the integrand at $s = s^*$, where we recall from Eq. (18) that s^* satisfies

$$s^* + r\, e^{-\sqrt{\frac{r+s^*}{D}}\, M} = 0 \;. \tag{34}$$

Evaluating the residue at the pole, we see that, up to pre-exponential factors, $Q_r(M, t)$ decays exponentially for large t as

$$Q_r(M, t) \sim e^{-\theta_r(M)\, t} \quad , \quad \text{where} \quad \theta_r(M) = -s^* \;. \tag{35}$$

It is easy to evaluate $\theta_r(M)$ as a function of M by solving Eq. (34) numerically. The asymptotic behaviors of $\theta_r(M)$ for small and large M are given by

$$\theta_r(M) \approx \begin{cases} r - \frac{r^2 M^2}{D} & , \quad M \to 0 \\[2ex] r\, e^{-\sqrt{\frac{r}{D}}\, M} & , \quad M \to \infty \;. \end{cases} \tag{36}$$

As the target recedes, i.e., M becomes large, the exponent $\theta_r(M)$ becomes exponentially small, indicating that the target survives longer, as expected. In this large M regime, Eq. (35) can be written in the form

$$Q_r(M, t) \approx \exp\left[-rt\, e^{-\sqrt{\frac{r}{D}}\, M}\right] = \exp\left[-e^{-\sqrt{\frac{r}{D}}\left(M - \sqrt{\frac{D}{r}}\, \ln(r\, t)\right)}\right] \;. \tag{37}$$

This is exactly the CDF of the Gumbel distribution in Eq. (22), associated with the typical fluctuations of the random variable M_t.

In the opposite limit $M \to 0$, the exponent $\theta_r(M)$ in Eq. (36) approaches a non-zero constant r. A priori, this may look a bit strange since one expects that $Q_r(M, t) \to 0$ as $M \to 0$ for any time t. Indeed, in Eq. (35), we have ignored pre-exponential factors. Taking into account these factors, it is easy to show that, as $M \to 0$,

$$Q_r(M, t) \approx e^{-r\, t}\, \frac{M}{\sqrt{\pi D\, t}} \;. \tag{38}$$

Thus $Q_r(M, t)$ indeed vanishes as $M \to 0$, but the exponent $\theta_r(M = 0) = r$ remains finite. Physically, this corresponds to Brownian trajectories that have not reset up to time t and have escaped in the direction opposite to the target. This is because if the trajectory resets even once, the target at $M = 0$ will not survive, since it is close to the resetting position at 0.

So far we have discussed the large t behavior of the survival probability $Q_r(M, t)$ for fixed M and we have seen that when $t = \mathcal{O}(e^{\sqrt{\frac{r}{D}} M})$, it acquires the form of the CDF of a Gumbel variable in Eq. (37). This corresponds to crossing the curve $M = \sqrt{D/r}\, \ln(r\, t)$ in the $M - t$ plane in Fig. (2). One can also analyse the behavior of $Q_r(M, t)$ for intermediate values of t, e.g., when $t = O(M)$. In this case, we use the large-deviation behavior of the PDF $P_r(M, t)$ in Eq. (32). Integrating over M gives

$$Q_r(M, t) \approx 1 - B\, e^{-t\, I\left(\frac{M}{t}\right)} \;, \tag{39}$$

where B is an unimportant pre-exponential factor (subleading for large t) and the rate function $I(z)$ is given in Eq. (33). When $t < M/\sqrt{4D\, r}$, i.e., $z = M/t > z_c = \sqrt{4Dr}$, one gets using Eq. (33)

$$Q_r(M, t) \approx 1 - B\, e^{-r\, t - \frac{M^2}{4D\, t}} \quad , \quad t < M/\sqrt{4D\, r} \;. \tag{40}$$
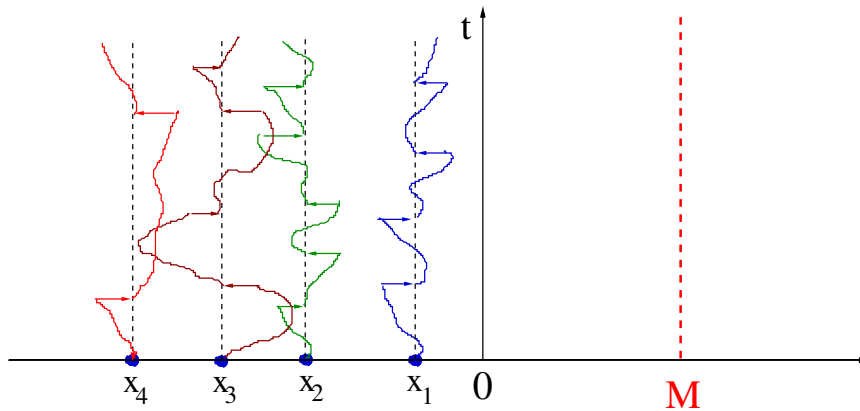
FIG. 4. Schematic trajectories of 4 independent resetting Brownian motions up to time t, each starting and resetting at $x_i \leq 0$ ($i = 1, 2, 3$ and 4). The target is located at $M > 0$ shown by the dashed red vertical line.

In contrast, when $t > M/\sqrt{4D\,r}$, but still $t \ll e^{\sqrt{\frac{r}{D}}M}$, using the first line of (33), one gets

$$Q_r(M,t) \approx 1 - B\,e^{-\sqrt{\frac{r}{D}}\,M} \ . \tag{41}$$

Thus in this regime the survival probability depends only weakly on time through the prefactor B. Finally, when t approaches $e^{\sqrt{\frac{r}{D}}M}$, it crosses over to the Gumbel form (37). To summarize, for fixed M and as a function of t, there are two time scales $t \sim O(M)$ and $t \sim e^{\sqrt{\frac{r}{D}}M}$, corresponding to crossing hirozontally the two lines in the $M - t$ plane in Fig. (2): the first time scale $t \sim O(M)$ corresponds to the regime of the large deviation of the EVS, while the second one corresponds to the regime of the typical behvaior of the EVS.

III.   MULTI-PARTICLE CASE

We now consider N independent RBMs, located initially on the negative half line with initial positions $\{x_i\}$ ($i = 1, 2, \ldots, N$). The i-th particle starts at x_i, undergoes independent diffusion and resets to x_i with rate r. The initial position x_i of the i-th particle is chosen independently from a uniform distribution over $x_i \in [-L, 0]$. We are interested in the thermodynamic limit when $N \to \infty$, $L \to \infty$, with the ratio $N/L = \rho$ fixed. For a fixed set of initial positions, we define M_t as the position of the global maximum of all N particles up to time t. Let us denote the CDF of M_t by $Q_r(M, t | \{x_i\}) = \text{Prob.}(M_t \leq M)$ for a given set of initial positions $\{x_i\}$'s. This CDF is also the survival probability of a fixed target located at M, see Fig. (4). Here, we can interpret this search process as a team-search by N independent walkers. The search terminates when any one of the N walkers finds the target for the first time.

Using the independence of N particles, the CDF for a fixed set of initial positions $\{x_i\}$'s is given by

$$Q_r(M, t | \{x_i\}) = \prod_{i=1}^{N} Q_r(M - x_i, t) \ , \tag{42}$$

where $Q_r(M, t)$ is the single particle CDF discussed in the previous section. Now we also need to average the survival probability in Eq. (42) with respect to the initial positions $\{x_i\}$'s, drawn independently from a uniform distribution. This averaging can be done in two different ways, namely (i) annealed and (ii) quenched, akin to disordered systems. In fact, this setup has been used to compute the current distribution in nonequilibrium systems of independent stochastic processes, such as for diffusive particles [65–70], for run-and-tumble particles [66, 68] and also for resetting Brownian motions [69]. More recently, the total number of visits to the origin by all particles up to time t (equivalently the local time at the origin for the combined N-particle process) has been computed for the similar step-like initial condition [71]. Here, we will use the formalism developed above and adapt it to study the survival probability, or equivalently the CDF of the maximum M_t. In the annealed case, one averages $Q_r(M, t | \{x_i\})$ in Eq. (42) directly, i.e.,

$$Q_{\text{an}}(M, t) = \overline{Q_r(M, t | \{x_i\})} = [Q_{\text{avg}}(M, t)]^N \ , \tag{43}$$

where

$$Q_{\text{avg}}(M,t) = \lim_{L\to\infty} \frac{1}{L} \int_{-L}^{0} Q_r(M - x, t)\, dx \tag{44}$$

where $\overline{\cdots}$ denotes the averaging over the initial positions $\{x_i\}$'s. In contrast, in the quenched case, one is interested in the typical initial configurations that dominate the survival probability. One way to extract the contribution from this typical initial configuration is to take the average over the logarithm of $Q_r(M, t|\{x_i\})$ and then re-exponentiate, i.e.,

$$Q_{\text{qu}}(M,t) = \exp\left[\overline{\ln Q_r(M, t|\{x_i\})}\right] . \tag{45}$$

It turns out that this is equivalent to choosing a specific initial configuration with equispaced points separated by $1/\rho$ [65, 66].

In the two sub-sections below, we discuss the annealed and the quenched cases separately.

A. Annealed case

In the annealed case, the survival probability or equivalently, the CDF $Q_{\text{an}}(M,t)$ is given by Eq. (43), where the average $\overline{\cdots}$ is over the initial positions $\{x_i\}$'s, each drawn independently and uniformly from $x_i \in [-L, 0]$. We first replace $Q_r(M - x_i, t)$ by $1 - (1 - Q_r(M - x_i, t))$ in Eq. (42) and average over $\{x_i\}$'s as in Eq. (43). This gives, using the independence of x_i's,

$$Q_{\text{an}}(M,t) = \left(1 - \frac{1}{L}\int_{-L}^{0} (1 - Q_r(M - x, t))\, dx\right)^N . \tag{46}$$

Changing varible $x \to -x_0$ and taking the thermodynamic limit $N \to \infty$, $L \to \infty$, with the ratio $N/L = \rho$ fixed, we get

$$Q_{\text{an}}(M,t) = \exp\left[-\rho \int_{0}^{\infty} (1 - Q_r(M + x_0, t))\, dx_0\right] . \tag{47}$$

We remark that the special case $M = 0$, i.e., the survival probability $Q_{\text{an}}(M = 0, t)$ for a target fixed at the origin was analysed in Ref. [26] with the interesting result that at long times, $Q_r(M = 0, t)$ decays algebraically as

$$Q_{\text{an}}(M = 0, t) \sim t^{-\theta}, \quad \theta = \rho\sqrt{\frac{D}{r}}, \tag{48}$$

with a continuously varying exponent θ. Here, our goal is to go beyond $M = 0$, and study the full CDF $Q_r(M, t)$ for all M.

To proceed for general $M \geq 0$, we rewrite Eq. (47) as

$$Q_{\text{an}}(M,t) = e^{-\rho J(M,t)} \quad , \quad \text{where} \quad J(M,t) = \int_{M}^{\infty} (1 - Q_r(x_0, t))\, dx_0 . \tag{49}$$

We then define the Laplace transform of $J(M,t)$ with respect to t as

$$\tilde{J}(M,s) = \int_{0}^{\infty} e^{-st} J(M,t)\, dt . \tag{50}$$

Taking the Laplace transform of $J(M,t)$ in Eq. (49) and using the single particle result in Eq. (14), we get

$$\tilde{J}(M,s) = \frac{\sqrt{D(r+s)}}{r\, s} \ln\left(1 + \frac{r}{s} e^{-\sqrt{\frac{r+s}{D}}M}\right) . \tag{51}$$

Using Bromwich inversion formula, we can write $J(M,t)$ formally as

$$J(M,t) = \int_{\Gamma} \frac{ds}{2\pi i}\, e^{st}\, \frac{\sqrt{D(r+s)}}{r\, s} \ln\left(1 + \frac{r}{s} e^{-\sqrt{\frac{r+s}{D}}M}\right) , \tag{52}$$
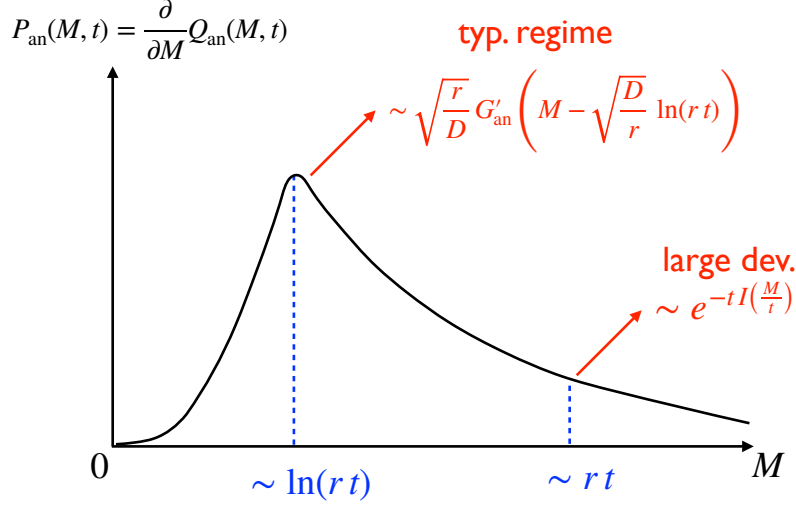
FIG. 5. A schematic plot of the annealed PDF $P_{\text{an}}(M,t)$ vs. M in Eq. (70). The two vertical dashed blue lines represent the typical and the large-deviation scales.

where Γ is the Bromwich contour.

Typical regime: In this case, we anticipate and verify a posteriori that the typical value of M_t scales as $\sqrt{D/r}\,\ln t$ for large t with $O(1)$ fluctuations around it. To extract this typical behavior from the Laplace transform in Eq. (52), we rescale $s\,t = \tilde{s}$ and re-write it as

$$J(M,t) = \sqrt{\frac{D}{r}} \int_\Gamma \frac{d\tilde{s}}{2\pi i} \frac{e^{\tilde{s}}}{\tilde{s}} \sqrt{1 + \frac{\tilde{s}}{rt}} \, \ln\left(1 + \frac{rt}{\tilde{s}} e^{-\sqrt{\frac{r + \frac{\tilde{s}}{t}}{D}} M}\right). \tag{53}$$

Now we take the $t \to \infty$ limit, $M \to \infty$ limit but keeping $M - \sqrt{D/r}\,\ln(rt) = z$ fixed. One immediately gets in this scaling limit

$$J(M,t) \approx F\left(M - \sqrt{\frac{D}{r}}\,\ln(rt)\right), \quad \text{where} \quad F(z) = \sqrt{\frac{D}{r}} \int_\Gamma \frac{d\tilde{s}}{2\pi i} \frac{e^{\tilde{s}}}{\tilde{s}} \, \ln\left(1 + \frac{1}{\tilde{s}} e^{-\sqrt{r/D}\,z}\right). \tag{54}$$

The scaling function $F(z)$ can be evaluated exactly by expanding the logarithm in the integrand in Eq. (54) in a power series in $1/\tilde{s}$ and then performing the Bromwich integral term by term. This gives

$$F(z) = -z + \sqrt{\frac{D}{r}}\left(\gamma_E + \Gamma\left(0, e^{-\sqrt{\frac{r}{D}}z}\right)\right), \tag{55}$$

where $\Gamma(0,u) = \int_u^\infty \frac{e^{-x}}{x}\,dx$ is the incomplete Gamma function. In particular, the asymptotic behaviors of $F(z)$ are given by

$$F(z) \approx \begin{cases} -z + \sqrt{\frac{D}{r}}\,\gamma_E, & z \to -\infty \\[2ex] \sqrt{\frac{D}{r}}\,e^{-\sqrt{\frac{r}{D}}z} & z \to +\infty. \end{cases} \tag{56}$$

Then using Eq. (49), we finally obtain our main result

$$Q_{\text{an}}(M,t) = e^{-\rho\,F\left(M - \sqrt{\frac{D}{r}}\,\ln(rt)\right)}. \tag{57}$$

Thus the CDF of M_t has the final scaling form

$$Q_{an}(M, t) \approx G_{an}\left(M - \sqrt{\frac{D}{r}}\ln(rt)\right) \tag{58}$$

$$\text{where} \quad G_{an}(z) = e^{-\rho F(z)} = \exp\left[-\rho\sqrt{\frac{D}{r}}\gamma_E + \rho z - \rho\sqrt{\frac{D}{r}}\Gamma\left(0, e^{-\sqrt{\frac{r}{D}}z}\right)\right]. \tag{59}$$

This function $G_{an}(z)$ is a new scaling function, different from the standard Gumbel form. Note that in the limit of large M, i.e., as $z \to \infty$, using the second line in Eq. (56), we get

$$G_{an}(z) \approx e^{-\rho\sqrt{\frac{D}{r}}e^{-\sqrt{r/D}z}}, \tag{60}$$

representing typically the Gumbel-like behavior of the CDF. In the opposite limit when $M \to 0$, i.e., when $z \to -\infty$, we get from the first line of (56)

$$Q_{an}(M \to 0, t) \sim e^{-\rho\sqrt{D/r}\ln(rt)} \sim t^{-\rho\sqrt{r/D}}, \tag{61}$$

thus recovering the known result (48) of Ref. [26]. As M increases from 0, our main new result in Eq. (58) thus interpolates smoothly between $M = 0$ and the typical value of $M \sim \sqrt{D/r}\ln t$. Finally, it follows that in this typical regime, the PDF

$$P_{an}(M, t) = \frac{\partial}{\partial M}Q_{an}(M, t), \tag{62}$$

has the scaling behavior

$$P_{an}(M, t) \approx G'_{an}\left(M - \sqrt{\frac{D}{r}}\ln(rt)\right), \tag{63}$$

where $G'(z) = dG/dz$ is the derivative of the scaling function $G(z)$ in Eq. (58).

Large-deviation regime: We start from Eq. (49) where $J(M, t)$ is given explicitly by Eq. (52). Note that the result in Eq. (52) is valid for all M. For the typical fluctuations, we considered the scaling limit $M \to \infty$, $t \to \infty$ with $M - \sqrt{D/r}\ln t = z$ fixed. For the large-deviation regime, when M is very large, one can expand the logarithm in (52) and only keep the first term, resulting in

$$J(M, t) \approx \int_\Gamma \frac{ds}{2\pi i} e^{st} \frac{\sqrt{D(r + s)}}{s^2} e^{-\sqrt{\frac{r+s}{D}}M}. \tag{64}$$

The integrand has a double pole at $s = 0$ and a brnach cut at $s = -r$. In addition it has a saddle point at $s_1 = -r + (M/t)^2/(4D)$ as in Eq. (20). If $s_1 > 0$, the dominant contribution to the integral comes from the saddle point, and evaluating this saddle point one gets the large deviation behavior $J(M, t) \approx e^{-rt - M^2/(4Dt)}$. The condition $s_1 > 0$ translates into $M > M_c(t)$ where

$$M_c(t) = \sqrt{4\,D\,r}\,t. \tag{65}$$

When $M < M_c(t)$, the double pole at $s = 0$ dominates and one gets $J(M, t) \approx t\,e^{-\sqrt{\frac{r}{D}}M}$. Thus, in the large-deviation regime when $M = O(t)$, we can combine the behaviors for $M < M_c(t)$ and $M > M_c(t)$ into a single large-deviation form

$$J(M, t) \approx e^{-t\,I\left(\frac{M}{t}\right)} \quad, \quad I(z) = \begin{cases} \sqrt{\frac{r}{D}}\,z, & z < z_c = \sqrt{4\,D\,r} \\ \\ r + \frac{z^2}{4D}, & z > z_c = \sqrt{4\,D\,r}. \end{cases} \tag{66}$$

The rate function $I(z)$ is identical to the single particle case in Eq. (33) and thus exhibits a second-order dynamical phase transition at $z = \sqrt{4\,D\,r}$. Hence, in this large-deviation regime, using Eqs. (49) and (66) we get the annealed CDF

$$Q_{an}(M, t) \approx \exp\left[-\rho e^{-t\,I\left(\frac{M}{t}\right)}\right] \approx 1 - \rho e^{-t\,I\left(\frac{M}{t}\right)}. \tag{67}$$

Another alternative way to analyse the large-deviation regime is by probing directly the annealed PDF in Eq. (62). Taking derivative of Eq. (49) with respect to M gives the exact expression

$$P_{\mathrm{an}}(M,t) = \rho \left[1 - Q_r(M,t)\right] e^{-\rho\,J(M,t)}\,. \tag{68}$$

We now substitute in Eq. (68) the large-deviation behavior of $Q_r(M,t)$ in Eq. (39) and that of $J(M,t)$ in Eq. (66). This leads for large t, large M but with M/t fixed, the following large-deviation behavior of $P_{\mathrm{an}}(M,t)$ (up to pre-exponential fcators)

$$P_{\mathrm{an}}(M,t) \sim e^{-t\,I\left(\frac{M}{t}\right)}\,, \tag{69}$$

with the rate function $I(z)$ given in Eq. (33).

Thus, to summarize, we find that in the annealed case, there are essentially two scales of M, namely $M \sim \sqrt{D/r}\,\ln(rt)$ characterzing typical flctuations and $M \sim t$ characterizing atypically large fluctuations. The behavior of the PDF of the maximum, for large t, can be summarized as

$$P_{\mathrm{an}}(M,t) \approx
\begin{cases}
G'_{\mathrm{an}}\left(M - \sqrt{\frac{D}{r}}\,\ln(rt)\right)\,, & \text{when} \quad M \sim \sqrt{\frac{D}{r}}\,\ln(rt)\,,\\[14pt]
e^{-t\,I\left(\frac{M}{t}\right)}\,, & \text{when} \quad M \sim t\,,
\end{cases} \tag{70}$$

with $G(z)$ and $I(z)$ given respectively in Eqs. (58) and (33) A schematic plot of $P_{\mathrm{an}}(M,t)$, in the typical and in the large-deviation regimes, is shown in Fig. 5.

B. Quenched case

In the quenched case, the survival probability or equivalently, the CDF $Q_{\mathrm{qu}}(M,t)$ is given by Eq. (45), where the average $\overline{\cdots}$ is again over the initial positions $\{x_i\}$'s, each drawn independently and uniformly from $x_i \in [-L,0]$. Performing this average (by changing $x_i \to -x_i$) and taking the thermodynamic limit gives

$$Q_{\mathrm{qu}}(M,t) = \exp\left[\overline{\ln Q_r(M,t|\{x_i\})}\right] = \exp\left[\frac{1}{L}\sum_{i=1}^{N}\int_{-L}^{0}\ln\left[Q_r(M-x_i,t)\right]dx_i\right] = \exp\left[\rho\int_{0}^{\infty}\ln\left[Q_r(M+x,t)\right]dx\right]\,. \tag{71}$$

Shifting x by $M+x$ in the integrand gives

$$Q_{\mathrm{qu}}(M,t) = \exp\left[\rho\int_{M}^{\infty}\ln\left[Q_r(m,t)\right]dm\right]\,, \tag{72}$$

where we recall that $Q_r(m,t)$ is the single particle survival probability with a target fixed at m, and is given by Eq. (15), i.e.,

$$Q_r(m,t) = \int_{\Gamma}\frac{ds}{2\pi i}\,e^{s\,t}\,\frac{1 - e^{-\sqrt{\frac{r+s}{D}}\,m}}{s + r\,e^{-\sqrt{\frac{r+s}{D}}\,m}} \tag{73}$$

Once again, the special case $M = 0$, i.e., the quenched survival probability $Q_{\mathrm{qu}}(M=0,t)$ for a target fixed at the origin was studied in Ref. [26] and it was found to decay exponentially for large t as

$$Q_{\mathrm{qu}}(M=0,t) \approx \exp\left[-\rho\sqrt{r\,D}\,\theta_1\,t\right]\,, \quad \text{with} \quad \theta_1 = 4(1 - \ln 2)\,. \tag{74}$$

Note that in Ref. [26], the exponent was $2\,\theta_1$ since the effective density there was 2ρ. Our goal here is to study $Q_{\mathrm{qu}}(M,t)$ for all $M \geq 0$, going beyond the special case $M = 0$.

To make progress for general $M \geq 0$, we first note that for large t, the dominant behavior of the integral in Eq. (73) is governed by the pole of the integrand and one has, to leading order for large t (ignoring pre-exponential factors),

$$Q_r(m,t) \approx e^{s^*(m)\,t}\,, \tag{75}$$

where the pole $s^*(m)$ satisfies

$$s^*(m) + r\,e^{-\sqrt{\frac{(r+s^*(m))}{D}}\,m} = 0\,. \tag{76}$$

Substituting (75) in Eq. (72) gives, up to pre-exponential factors,

$$Q_{\text{qu}}(M,t) \approx \exp\left[\rho\, t \int_M^\infty s^*(m)\, dm\right].$$ (77)

The pole $s^*(m)$ in Eq. (76) is necessarily negative. It is then natural to substitute $s^*(m) = -r\, y$ in Eq. (77) such that $y \geq 0$. Under this substitution, it follows from Eq. (76) that the variable y satisfies

$$y = e^{-\sqrt{\frac{r}{D}(1-y)}\, m}, \quad \text{implying} \quad m = -\sqrt{\frac{D}{r}}\, \frac{\ln y}{\sqrt{1-y}}.$$ (78)

We now make the change of variable $m \to y$ in Eq. (77) and obtain, using (78)

$$Q_{\text{qu}}(M,t) \approx \exp\left[-\rho\, \sqrt{r\, D}\, t\, W\left(\sqrt{\frac{r}{D}}\, M\right)\right].$$ (79)

Here the function $W(u)$ is given by

$$W(u) = \int_0^{y^*(u)} \left[\frac{1}{\sqrt{1-y}} + \frac{y\, \ln y}{2\,(1-y)^{3/2}}\right] dy,$$ (80)

where $0 \leq y^*(u) \leq 1$ is determined in terms of u by solving the equation

$$y^*(u) = e^{-\sqrt{1-y^*(u)}\, u}.$$ (81)

It turns out that the integral in Eq. (80) can be performed explicitly, giving

$$W(u) = 4\left(1 - \sqrt{1-y^*}\right) + 4\left[\text{arctanh}\left(\sqrt{1-y^*}\right) - \ln 2\right] + \frac{(2-y^*)\, \ln(y^*)}{\sqrt{1-y^*}},$$ (82)

with $y^* \equiv y^*(u)$ determined from Eq. (81) as a function of u. From Eq. (81), it is easy to derive the asymptotic behavior of $y^*(u)$. One gets

$$y^*(u) \approx \begin{cases} 1 - u^2, & \text{as} \quad u \to 0 \\[2mm] e^{-u}, & \text{as} \quad u \to \infty. \end{cases}$$ (83)

Consequently, the asymptotic behaviors of $W(u)$ in Eq. (82) are given by

$$W(u) \approx \begin{cases} 4\,(1 - \ln 2) - u, & \text{as} \quad u \to 0 \\[2mm] e^{-u}, & \text{as} \quad u \to \infty. \end{cases}$$ (84)

A plot of the function $W(u)$, obtained using Mathematica, is provided in Fig. (6). Substituting the $W(u \to 0)$ behavior above in Eq. (79), we reproduce the $M \to 0$ limit of $Q_{\text{qu}}(M = 0, t)$ in Eq. (74). On the other hand, substituting the large u behavior of $W(u) \approx e^{-u}$ in Eq. (79), we see that a natural scaling limit emerges: $M \to \infty$, $t \to \infty$ but with $M - \sqrt{D/r}\, \ln(rt) = z$ fixed. This is indeed the typical behvaior of $Q_{\text{qu}}(M,t)$.

Typical regime: In this typical scaling regime, where M and t are both large with $M - \sqrt{D/r}\, \ln(rt) = z$ fixed, we then get from Eq. (79)

$$Q_{\text{qu}}(M,t) \approx G_{\text{qu}}\left(M - \sqrt{\frac{D}{r}}\, \ln(rt)\right), \quad \text{where} \quad G_{\text{qu}}(z) = \exp\left[-\rho\, \sqrt{\frac{D}{r}}\, e^{-\sqrt{r/D}\, z}\right].$$ (85)

One should compare this typical scaling behavior in the quenched case with that of the annealed case in Eq. (58). While in the annealed case, the scaling function $G_{\text{an}}(z)$ is a new function not of the Gumbel form, in the quenched case the scaling function $G_{\text{qu}}(z)$ in Eq. (85) has a Gumbel form. Another difference between the two cases is worth remarking. In the annealed case, the very small M behavior ($M \to 0$) is included in the scaling form in Eq. (58) corresponding to the $z \to -\infty$ limit. In contrast, in the quenched case, the $M \to 0$ limit in Eq. (74) is not part of the scaling function $G_{\text{qu}}(z)$ in Eq. (85). To see this, we note that substituting $M = 0$, i.e., $z = -\sqrt{\frac{D}{r}}\, \ln(rt)$ in Eq. (85)
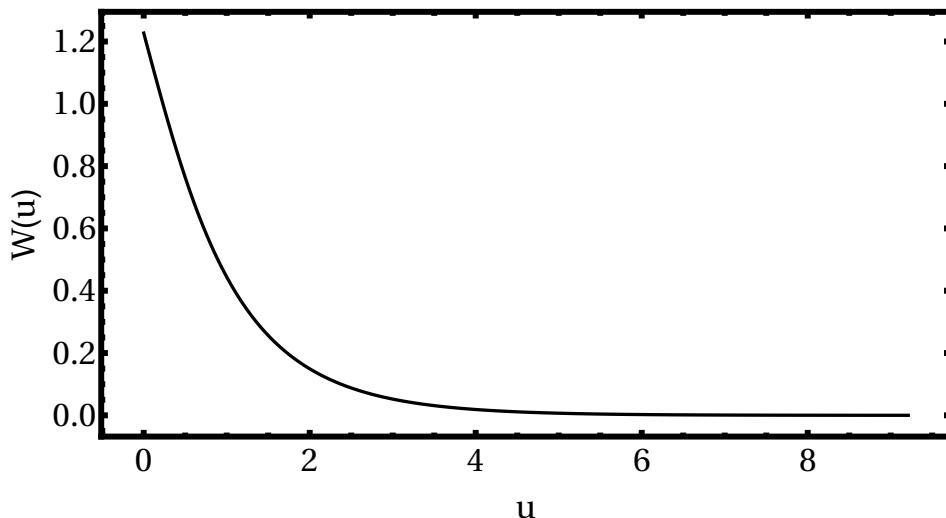
FIG. 6. The function $W(u)$ vs. u obtained by eliminating $y^*(u)$ between Eqs. (82) and (81) using Mathematica. The function $W(u) \to 4(1 - \ln 2) = 1.22741 \cdots$ as $u \to 0$ and decays exponentially as $W(u) \approx e^{-u}$ as $u \to \infty$ as described in Eq. (84).

gives, $Q_{\mathrm{qu}}(0,t) \approx \exp[-\rho \sqrt{D \, r} \, t]$ which is different from the true $M = 0$ behavior in Eq. (74). In the quenched case, the behavior of $Q_{\mathrm{qu}}(M,t)$, for both small and large $M \sim O(\ln(rt))$, is rather captured by the result in Eq. (79) with the function $W(u)$ given explicitly in Eqs. (82) and (81).

Large-deviation regime: In the discussion about typical fluctuations above we probed the CDF $Q_{\mathrm{qu}}(M,t)$ as a function of M, for fixed large t, at the scale $M \sim \sqrt{D/r} \ln t$. Let us now investigate the same CDF $Q_{\mathrm{qu}}(M,t)$ at the scale of large deviations when $M \sim O(t)$. As in the annealed case, to investigate this large-deviation regime, it is convenient to consider the PDF of M, namely,

$$P_{\mathrm{qu}}(M,t) = \frac{\partial}{\partial M} Q_{\mathrm{qu}}(M,t). \tag{86}$$

Taking derivative of Eq. (72) with respect to M yields the exact PDF

$$P_{\mathrm{qu}}(M,t) = -\rho \ln \left[Q_r(M,t) \right] \exp \left[\rho \int_M^\infty \ln \left[Q_r(m,t) \right] dm \right], \tag{87}$$

where $Q_r(m,t)$ is the single particle CDF given in Eq. (73). In the large-deviation regime when $M \sim O(t)$, we then use the large-deviation result for $Q_r(M,t)$ in Eq. (39). Substituting this result in Eq. (87) and taking the limit $t \to \infty$, it is straightforward to see that the exponential factor in Eq. (87) contributes 1 to leading order and expanding the logarithm in the front one gets, to leading order for large t (ignoring pre-exponential factors as usual)

$$P_{\mathrm{qu}}(M,t) \approx e^{-t \, I\left(\frac{M}{t}\right)}, \tag{88}$$

where the rate function $I(z)$ is given exactly in Eq. (33). The second derivative of the rate function $I(z)$ is discontinuous at $z = z_c = \sqrt{4Dr}$, signalling a second-order phase transition. The result for the quenched case in Eq. (88) is identical (up to pre-exponential factors) to that in the annealed case in Eq. (69). Thus, on the scale $M \sim O(t)$, both the annealed and the quenched PDF's of M, respectively in Eqs. (69) and (88), are described by an identical large-deviation form that coincides with the single particle case in Eq. (32).

Thus, in the quenched case, the behavior of $Q_{\mathrm{qu}}(M,t)$ or equivalently the PDF $P_{\mathrm{qu}}(M,t) = \partial_M Q_{\mathrm{qu}}(M,t)$ can be summarized as follows (ignoring pre-exponential factors as usual)

$$P_{\mathrm{qu}}(M,t) \approx \begin{cases} \exp\left[-\rho \sqrt{r \, D} \, t \, W\left(\sqrt{\frac{r}{D}} M \right) \right], & \text{when } M \sim \sqrt{\frac{D}{r}}, \\[2ex] G'_{\mathrm{qu}}\left(M - \sqrt{\frac{D}{r}} \ln(rt) \right), & \text{when } M \sim \sqrt{\frac{D}{r}} \ln(rt), \\[2ex] e^{-t \, I\left(\frac{M}{t}\right)}, & \text{when } M \sim t, \end{cases} \tag{89}$$

where the functions $W(u)$, $G_{\text{qu}}(z)$ and $I(z)$ are given respectively in Eqs. (82), (85) and (33). Thus, compared to the annealed case in Eq. (70), we see that in the quenched case there is an additional scale when $M \sim O(1)$ for large t, where the PDF $P_{\text{qu}}(M,t)$ behaves differently from the typical regime. This is natural because in the quenched case a scale of $O(1)$ naturally emerges from the initial condition where the particles are equispaced.

IV. NUMERICAL SIMULATIONS

To study the problem numerically [72], we start with the **single particle** case. To obtain a numerical approximation of the cumulative distribution $Q_r(M,t)$ at a fixed given time t, we considered an array $\overline{Q}(M,t')$ which is discretised in time with time resolution Δt, i.e., for $t' = 0, \Delta t, 2\Delta t, \ldots, t$. We applied a discretised version of Eq. (10) which reads

$$\overline{Q}(M,t') = e^{-rt'} Q_0(M,t') + (1 - e^{-r\Delta t}) \sum_{\tau = \Delta t, 2\Delta t, \ldots}^{t'} e^{-r(\tau - \Delta t)} \overline{Q}(M, t' - \tau) Q_0(M, \tau) \tag{90}$$

where the survival probability $Q_0(M,t)$ of an ordinary Brownian motion without resetting is given by Eq. (9) and e^{-r} is the probability of experiencing no reset in the unit time span. Thus, each term in the sum represents the case that a particle experiences the last reset at time $t' - \tau$, i.e., $\tau/\Delta t$ "steps" back in time, for all possible values of $\Delta t \leq \tau \leq t'$. This happens with the probability which is a product of the probability $(1 - e^{-r\Delta t})$ for the last reset times the probability $e^{-r(\tau - \Delta t)}$ for experiencing no reset since the last reset, during time $\tau - \Delta t$. For the calculation of $\overline{Q}(M,t')$ one includes the probabilities $\overline{Q}(M, t' - \tau)$ and $Q_0(M, \tau)$ that a particle does not reach position M in the both time intervals before and after the last reset, respectively.

To achieve a high numerical accuracy in evaluating very small probabilities like 100^{-100} and estimating the sums and differences of probabilities, we used the `mpfr` library [73, 74] with a precision of 1000 binary digits for storing data in arrays and performing arithmetic operations.

To estimate numerically the probability density, we approximate Eq. (6) by a finite difference

$$P_r(M,t) \approx \frac{\overline{Q}_r(M+h, t) - \overline{Q}_r(M-h, t)}{2h}. \tag{91}$$

Thus, to investigate $P_r(M,t)$ for a sequence $M = k\Delta M$ ($k = 1, 2, 3, \ldots$) of values of M, we actually considered the values $\Delta M - h, \Delta M + h, 2\Delta M - h, 2\Delta M + h, 3\Delta M - h, \ldots$. We tested different spacing values h and found no notable changes when going below $h = 0.01$.

Note that for $\Delta t \to 0$ the factor in front of the sum in Eq. (90) becomes $r\Delta t$ and $e^{-r(\tau - \Delta t)} \to e^{-r\tau}$, therefore one obtains Eq. (10). One can expect an influence of the discretisation but it will be small, because quantities like the survival probability $Q_0(M, \tau)$ and the no-reset probability $e^{-rt'}$ are always exact independently of the choice of Δt. We have tested this explicitly by calculating the single-particle distribution $P_r(M,t)$ for various values of Δt, here for the parameter values $t = 1000$, $D = 1$ and $r = 0.1$. The result is shown in Fig. 7. For values below $\Delta t = 2$ we observed no significant change in the results in Fig. 7, so we kept $\Delta t = 1$ throughout our study.

Having tested the dependence on Δt of $P_m(M,t)$ in Fig. 7, we then fix $\Delta t = 1$ and present the result for the single-particle distribution $P_r(M,t)$ vs. M in Fig. 8 for $t = 1000$ and compared it to the analytical result in Eq. (31). Generally, a very good agreement can be observed, for the left tail, the typical region, the intermediate region and for the large-deviation Gaussian tail. The predicted large-deviation behavior in Eq. (33) is confirmed by plotting the numerically obtained rate function $I(z) = -\log(P_r(M,t))/t$ as a function of $z = M/t$ in Fig. 9.

For the multi-particle **annealed case** we approximate the average in Eq. (44) of the single-particle cumulative function $Q_r(M,t)$ over all possible initial position in the interval $[-L, 0]$ by a finite sum over N evenly-spaced particle positions $x = -(N-1)\delta, -(N-2)\delta, \ldots, \delta, 0$. The particles exhibit a density $\rho = N/L$, i.e., the spacing is $\delta = L/N$. In the present work we use $\delta = 1$. Since starting at position $-i\delta$ and reaching a maximum M is equivalent to start at position 0 with reaching a maximum $M + i\delta$, one obtains

$$Q_{\text{avg}}(M,t) \approx \frac{1}{N} \sum_{i=0}^{N-1} Q_r(M + i\delta, t). \tag{92}$$

Note that the spacing of the considered values of M must be such that it is compatible with the needed values $M + i\delta$. For any target value of M, we also perform the full calculation for $M - h$ and $M + h$.

The cumulative distribution in Eq. (46) for the annealed case is simply $[Q_{\text{avg}}(M,t)]^N$ from Eq. (43), therefore $P_{\text{an}}(M,t) = \frac{\partial}{\partial M}[Q_{\text{avg}}(M,t)]^N = N\frac{\partial Q_{\text{avg}}(M,t)}{\partial M}[Q_{\text{avg}}(M,t)]^{N-1}$. The partial derivative is again obtained by taking the
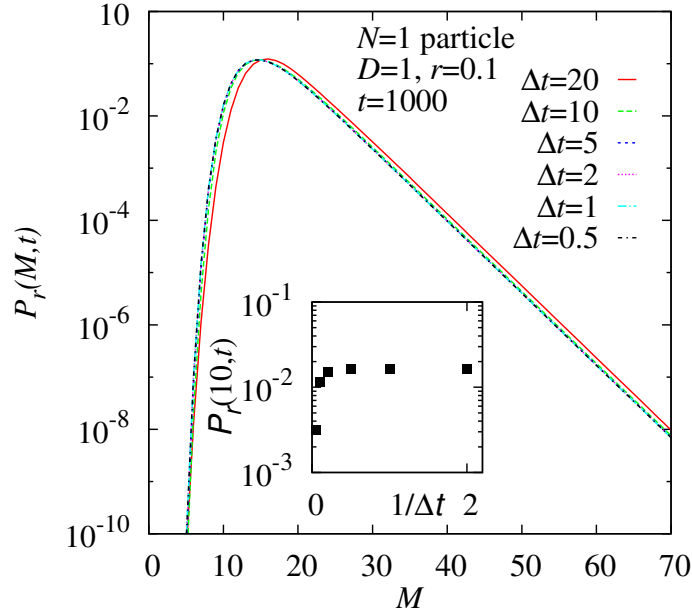
FIG. 7. One-particle distribution $P_r(M,t)$ for $t = 1000$, $D = 1$, $r = 0.1$ and various values Δt of the discretisation in time. The inset shows how the particular value $P_r(10,t)$ depends on $1/\Delta t$.
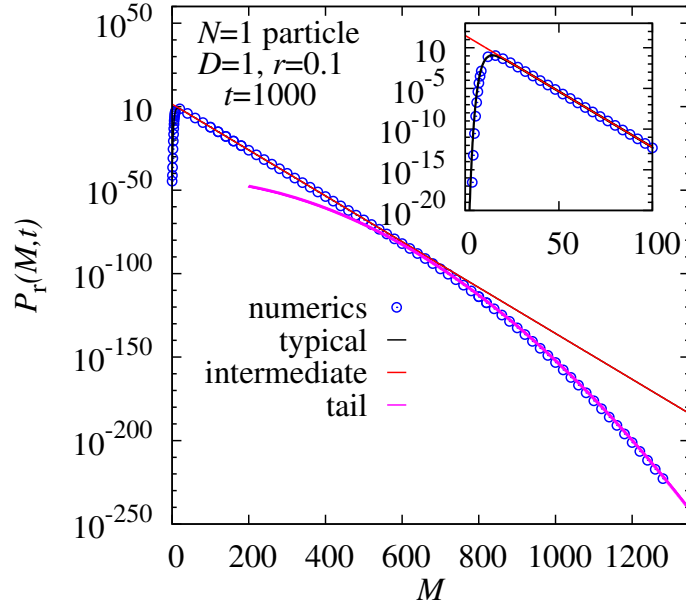

FIG. 8. Numerical one-particle distribution $P_r(M,t)$ for $t = 1000$, $D = 1$, $r = 0.1$ (symbols) compared to the analytical result in Eq. (31) (lines). The inset highlights the range of small values of M.

numerical difference in Eq. (91). The result for the numerical density is then given by

$$P_{\mathrm{an}}(M,t) \approx N \frac{Q_{\mathrm{avg}}(M+h,t) - Q_{\mathrm{avg}}(M-h,t)}{2h} [Q_{\mathrm{avg}}(M,t)]^{N-1} \tag{93}$$

The resulting distribution for $N = 100$ particles in interval $[-(N-1), 0]$ with spacing $\delta = 1/\rho = 1$ is shown in Fig. 10. We tested that increasing the number N of particles does not change the result, the additional particles are just too far away. The numerical results confirm very well the analytical results in Eq. (70), for the typical region, as well as for the tail which is governed again by the rate function $I(z)$.

For the multi-particle **quenched case**, we consider just one configuration of particles at positions $x = -(N -$
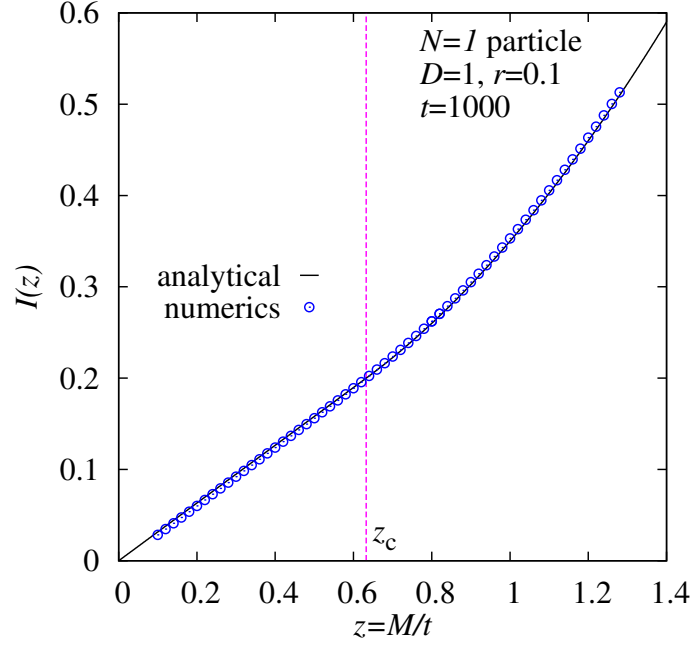
FIG. 9. Numerical result for the one-particle rate function $I(z)$ for $t = 1000$, $D = 1$, $r = 0.1$ (symbols) compared to the analytical result of Eq. (33) (solid line). The red vertical line provides the location of the critical value $z_c = \sqrt{4D\,r} = 0.632456\ldots$.
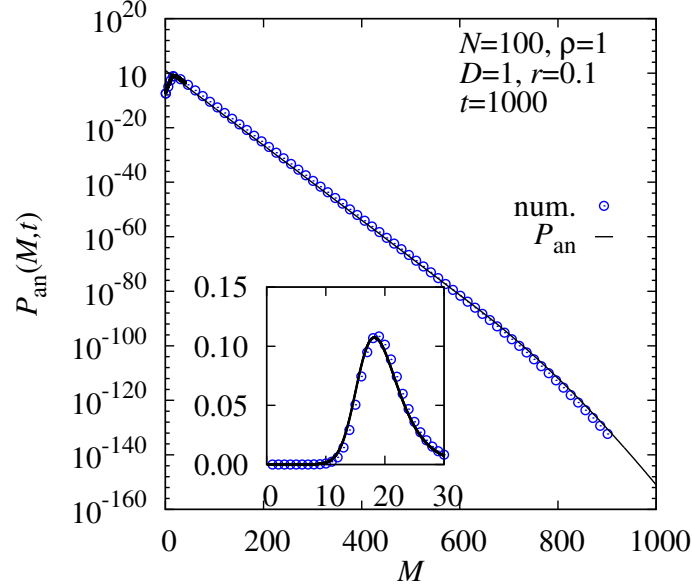

FIG. 10. Numerical result for the annealed distribution $P_{\mathrm{an}}(M, t)$ for $t = 1000$, $D = 1$, $r = 0.1$ and $N = 100$ particles (symbols). The lines show the analytical result in Eq. (70). The inset highlights the typical region in the first line of Eq. (70).

$1)\delta, -(N-2)\delta, \ldots, \delta, 0$. Therefore, the cumulative distribution is given by

$$Q_{\mathrm{qu}}(M, t) = \prod_{i=0}^{N-1} Q_r(M + i\delta, t) \,. \tag{94}$$

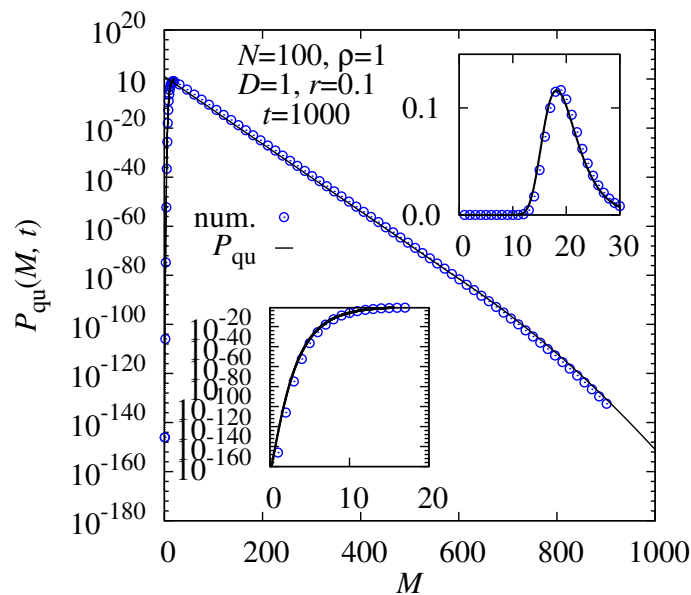To obtain the density, we take the derivative with respect to M and approximate the derivative of the single-particle

FIG. 11. Numerical result for the quenched distribution $P_{\rm qu}(M, t)$ for $t = 1000$, $D = 1$, $r = 0.1$ and $N = 100$ particles (symbols). The lines show the analytical result in Eq. (89). The inset in the upper right corner highlights the typical regime (as given by the second line of Eq. (89)). The inset in the lower left corner corresponds to the left tail, when $M \sim \sqrt{D/r}$, as given in the first line of Eq. (89).

cumulative distribution again by a finite difference arriving at

$$
P_{\rm qu}(M, t) = \sum_{i=0}^{N-1} \frac{Q_r(M + i\delta + h, t) - Q_r(M + i\delta - h, t)}{2h} \prod_{j=0, j \neq i}^{N-1} Q_r(M + j\delta, t). \tag{95}
$$

The resulting distribution for the quenched case for $N = 100$ particles in interval $[-(N-1), 0]$ with density $\rho = 1$ is shown in Fig. 11. Also here, the numerical results confirm very well the analytical results in Eq. (89), for the typical region, for both tails and for the intermediate region.

V. CONCLUSION

In this paper, we first revisited the exact computation of the probability distribution of the maximum M_t of a single resetting Brownian motion (RBM) of duration t, starting and resetting at the origin with a constant rate r. In this case, it was known that the random variable M_t fluctuates around $\sqrt{D/r} \ln(r\,t)$ for large t and the typical scale of fluctuations is of order $O(1)$. The appropriately centered and scaled distribution of M_t approaches at large times to a standard Gumbel distribution. In this paper, we have analysed the large-deviation regime of M_t when $M_t \sim O(t)$ and shown that its PDF satisfies a large-deviation form $P_r(M, t) \sim e^{-tI(M/t)}$ where the rate function $I(z)$ has a second-order discontinuity at the critical value $z_c = \sqrt{4D\,r}$. This signals a dynamical phase transition in the tail of the distribution of the maximum. Next, we considered a collection of independent RBMs with initial (and resetting) positions uniformly distributed with a density ρ over the negative half-line. In this case, the distribution of the global maximum up to time t depends on how one carries out the average over the initial positions. In the annealed case the stochastic trajectories and the initial positions are averaged simultaneously, while in the quenched case, one averages only over the stochastic trajectories for a fixed initial condition, which is a typical one, i.e., the initial condition that has the largest probability of occurrence. In the annealed case, we showed that the PDF of the maximum, appropriately centered around $\sqrt{D/r} \ln(r\,t)$ and scaled by a constant factor, approaches at late times to a new limiting distribution characterized by a scaling function $G'_{\rm an}(z)$, which is different from the well known Gumbel law for a single particle. Thus, even though the particles are independent, the averaging over the initial positions modifies the typical distribution of the maximum. However, the large-deviation behaviour of M_t when $M \sim O(t)$ remains the same as the single particle case. Hence, in the annealed case, the fluctuations of the initial positions modify the typical behavior of the maximum, but not its large-deviation tails. In contrast, for the quenched case, we showed that the PDF of the maximum, centered at $\sqrt{D/r} \ln(r\,t)$ and scaled by a constant, does approach the limiting

Gumbel form, but with nontrivial large-deviation tails on both sides of the typical value, i.e., both when $M \sim O(1)$ and $M \sim O(t)$. Thus in the quenched case, the fluctuations of the initial positions affect only the large-deviation behavior of M_t. Our analytical predictions, both for the typical as well as for the large-deviation regime of M_t, have been verified numerically to a very high precision, down to 10^{-250} for the PDF of M_t.

There are many directions in which this work can be extended. Here we considered independent RBMs distributed initially over the semi-infinite space. Recently, another model of resetting Brownian motions has been introduced where the position of the walkers are simultaneously reset to their initial positions but they evolve independently between two resetting events [75, 76]. Simultaneous resetting makes the positions of the particles correlated and it would be interesting to study the distribution of M_t in this correlated case with the semi-inifinite initial conditions as studied in this paper for independent RBMs. Another interesting extension would be to study the distribution of the extremes (both the maximum as well as the minimum) for a set of RBMs in higher dimensions with initial positions distributed uniformly over a given region of space.

ACKNOWLEDGMENTS

[1] W. J. Bell *Searching Behaviour: The Behavioural Ecology of Finding Resources* (London: Chapman and Hall, 1991).

[2] G. M. Viswanathan, M. G. E. da Luz, E. P. Raposo, H. E. Stanley *The Physics of Foraging: An Introduction to Random Searches and Biological Encounters* (Cambridge: Cambridge University Press, 2011).

[3] O. G. Berg, R. B. Winter, P. H. von Hippel, Biochemistry, **20**, 6929 (1981).

[4] S. Condamin, O. Bénichou, V. Tejedor, R. Voituriez, J. Klafter, Nature, **450**, 77 (2007).

[5] G. Oshanin, K. Lindenberg, H. S. Wio, S. Burlatsky, J. Phys. A: Math. Theor. **42**, 434008 (2009).

[6] P. L. Krapivsky, S. N. Majumdar, A. Rosso, J. Phys. A: Math. Theor. **43**, 315001 (2010).

[7] O. Bénichou, C. Loverdo, M. Moreau, R. Voituriez Rev. Mod. Phys. **83**, 81 (2011).

[8] B. Meerson, S. Redner, Phys. Rev. Lett. **114**, 198101 (2015).

[9] A. Godec, R. Metzler, Scientific reports, **6**, 20349 (2016).

[10] A. Godec, R. Metzler, Phys. Rev. X, **6**, 041037 (2016).

[11] D. S. Grebenkov, G. Oshanin, Phys. Chem. Chem. Phys. **19**, 2723 (2017).

[12] D. S. Grebenkov, R. Metzler, G. Oshanin, New J. Phys. **21**, 122001 (2019).

[13] G. Maercado-Vásquez, D. Boyer, Phys. Rev. Lett. **123**, 250603 (2019).

[14] W. Feller, *Introduction to Probability Theory and Its Applications*, Vol. 2 (Wiley: New York, 1966).

[15] S. Redner, A Guide to First-Passage Processes (Cambridge University Press, Cambridge, UK, 2007).

[16] S. N. Majumdar, Curr. Sci. **77**, 370 (1999).

[17] S. N. Majumdar, Curr. Sci. **89**, 2076 (2005).

[18] A. J. Bray, S. N. Majumdar, G. Schehr, Adv. Phys. **62**, 225 (2013).

[19] R. Metzler, S. Redner, G. Oshanin, *First-passage phenomena and their applications* (World Scientific), **35** (2014).

[20] E. J. Gumbel, *Statistics of Extremes* (Dover, New York, 1958).

[21] R. W. Katz, M. B. Parlange, P. Naveau, *Statistics of extremes in hydrology*, Adv. Wat. Res., **25**, 1287 (2002).

[22] S. Y. Novak, *Extreme value methods with applications to finance* (CRC Press, 2011).

[23] M. R. Leadbetter, G. Lindgren, H. Rootzén, *Extremes and related properties of random sequences and processes* (Springer Science & Business Media, 2012).

[24] S. N. Majumdar, A. Pal, G. Schehr, Phys. Rep. **840**, 1 (2020).

[25] S. Redner, M. R. Petersen, Phys. Rev. E **74**, 061114 (2006).

[26] M. R. Evans, S. N. Majumdar, Phys. Rev. Lett. **106**, 160601 (2011).

[27] M. R. Evans, S. N. Majumdar, J. Phys. A: Math. Theor. **44**, 435001 (2011).

[28] M. R. Evans, S. N. Majumdar, J. Phys. A: Math. Theor. **47**, 285001 (2014).

[29] A. Nagar, S. Gupta, Phys. Rev. E **93**, 060102 (R) (2016).

[30] A. Pal, A. Kundu, and M. R. Evans, J. Phys. A: Math. Theor. **49**, 225001 (2016).

[31] U. Bhat, C. De Bacco, and S. Redner, J. Stat. Mech. 083401 (2016).

[32] A. Pal, S. Reuveni, Phys. Rev. Lett. **118**, 030603 (2017).

[33] I. Eliazar and S. Reuveni, J. Phys. A: Math. Theor. **53**, 405004 (2020).

[34] L. Kusmierz, S. N. Majumdar, S. Sabhapandit, G. Schehr, Phys. Rev. Lett. **113**, 220602 (2014).

[35] S. N. Majumdar, S. Sabhapandit, G. Schehr, Phys. Rev. E **91**, 052131 (2015).

[36] S. Reuveni, Phys. Rev. Lett. **116**, 170601 (2016).

[37] M. Montero, J. Villarroel, Phys. Rev. E **94**, 032132 (2016).

[38] A. Chechkin, I. M. Sokolov, Phys. Rev. Lett. **121**, 050601 (2018).

[39] P. C. Bressloff, J. Phys. A: Math. Theor. **53**, 425001 (2020).

[40] R. G. Pinsky, Stoch. Proc. Appl. **130**, 2954 (2020).

[41] B. De Bruyne, S. N. Majumdar, G. Schehr, Phys. Rev. Lett. **128**, 200603 (2022).

[42] C. Christou, A. Schadschneider, J. Phys. A: Math. Theor. **48**, 285003 (2015).

[43] D. Campos, V. Méndez, Phys. Rev. E **92**, 062115 (2015).

[44] S. Belan, Phys. Rev. Lett. **120**, 080601 (2018).

[45] S. Ray, D. Mondal, S. Reuveni, J. Phys. A: Math. Theor. **52**, 255002 (2019).

[46] S. Ahmad, I. Nayak, A. Bansal, A. Nandi, D. Das, Phys. Rev. E **99**, 022130 (2019).

[47] A. Pal, V. V. Prasad, Phy. Rev. Research **1**, 032001 (2019).

[48] A. Pal, V. V. Prasad, Phys. Rev. E. **99** 032123 (2019).

[49] G. Mercado-Vsquez, D. Boyer, S. N. Majumdar, G. Schehr, J. Stat. Mech., 113203 (2020).

[50] G. Mercado-Vsquez, D. Boyer, S. N. Majumdar, J. Stat. Mech., 063203 (2022).

[51] G. Mercado-Vsquez, D. Boyer, S. N. Majumdar, J. Stat. Mech., 093202 (2022).

[52] M. Biroli, S. N. Majumdar, G. Schehr, Phys. Rev. E **107**, 064141 (2023).

[53] M. R. Evans, S. N. Majumdar, and G. Schehr, J. Phys. A **53**, 193001 (2020).

[54] A. Pal, S. Kostinski, S. Reuveni, J. Phys. A: Math. Theor. **55**, 021001 (2022).

[55] S. Gupta, A. M. Jayannavar, Frontiers in Physics **10**, 789097 (2022).

[56] O. Tal-Friedman, A. Pal, A. Sekhon, S. Reuveni, Y. Roichman, J. Phys. Chem. Lett. **11**, 7350 (2020).

[57] B. Besga, A. Bovon, A. Petrosyan, S. N. Majumdar, S. Ciliberto, Phys. Rev. Research **2**, 032029(R) (2020).

[58] B. Besga, F. Faisant, A. Petrosyan, S. Ciliberto, and S.N. Majumdar, Phys. Rev. E **104**, L012102 (2021).

[59] F. Faisant, B. Besga, A. Petrosyan, S. Ciliberto, S. N. Majumdar, J. Stat. Mech., 113203 (2021).

[60] M. Biroli, F. Mori, S. N. Majumdar, J. Phys. A: Math. Theor. **55**, 244001 (2022).

[61] S. N. Majumdar, F. Mori, H. Schawe, G. Schehr, Phys. Rev. E **103**, 022135 (2021).

[62] F. Mori, S. N. Majumdar, G. Schehr, Europhys. Lett. **135**, 30003 (2021).

[63] F. Mori, S. N. Majumdar and G. Schehr, Phys. Rev. E **106**, 054110 (2022).

[64] P. Singh and A. Pal, Phys. Rev. E **103**, 052119 (2021).

[65] B. Derrida, A. Gerschenfeld, J. Stat. Phys. **137**, 978 (2009).

[66] T. Banerjee, S. N. Majumdar, A. Rosso, G. Schehr, Phys. Rev. E **101**, 052101 (2020).

[67] S. Marbach, J. Chem. Phys. 154, 171101 (2021).

[68] T. Banerjee, R. L. Jack, M. E. Cates, Phys. Rev E **106**, L062101 (2022).

[69] C. Di Bello, A. K. Hartmann, S. N. Majumdar, F. Mori, A. Rosso, G. Schehr, Phys. Rev. E **108**, 014112 (2023).

[70] D. S. Dean, S. N. Majumdar, G Schehr, J. Stat. Mech. 063208 (2023).

[71] I. Burenev, S. N. Majumdar, A. Rosso, arXiv preprint: 2306.16882

[72] A.K. Hartmann, *Big Practical Guide to Computer Simulations*, World Scientific, Singapore (2015)

[73] MPFR multi precision floating point library, `https://www.mpfr.org/`

[74] L. Fousse, G. Hanrot, V. Lefèvre, P. Pélissier, and P. Zimmermann, ACM Trans. Math. Software **33**, 13es (2007)

[75] M. Biroli, H. Larralde, S. N. Majumdar, G. Schehr, Phys. Rev. Lett. **130**, 207101 (2023).

[76] M. Biroli, H. Larralde, S. N. Majumdar, G. Schehr, preprint arXiv:2307.15351.